Platform

SunCHECK®

One Database for Complete Quality Management

Learn more >

Patient

- Plan Quality Checks
- Secondary Dose Calculations
- Pre-Treatment QA
- In-Vivo Monitoring

Machine

- Standardized Routine QA
- Direct Device Control
- Automated Imaging, MLC & VMAT QA
- Protocol-Based QA

sunnuclear.com

SUN NUCLEAR
A MIRION MEDICAL COMPANY

MR to ultrasound image registration with segmentation-based learning for HDR prostate brachytherapy

Yizheng Chen, Lei Xing, Lequan Yu, Wu Liu, Benjamin Pooya Fahimian, Thomas Niedermayr, Hilary P. Bagshaw, Mark Buyyounouski and Bin Han[a)]
Department of Radiation Oncology, Stanford University, Stanford, CA 94305, USA

Purpose: Propagation of contours from high-quality magnetic resonance (MR) images to treatment planning ultrasound (US) images with severe needle artifacts is a challenging task, which can greatly aid the organ contouring in high dose rate (HDR) prostate brachytherapy. In this study, a deep learning approach was developed to automatize this registration procedure for HDR brachytherapy practice.

Methods: Because of the lack of training labels and difficulty of accurate registration from inferior image quality, a new segmentation-based registration framework was proposed for this multi-modality image registration problem. The framework consisted of two segmentation networks and a deformable registration network, based on the weakly -supervised registration strategy. Specifically, two 3D V-Nets were trained for the prostate segmentation on the MR and US images separately, to generate the weak supervision labels for the registration network training. Besides the image pair, the corresponding prostate probability maps from the segmentation were further fed to the registration network to predict the deformation matrix, and an augmentation method was designed to randomly scale the input and label probability maps during the registration network training. The overlap between the deformed and fixed prostate contours was analyzed to evaluate the registration accuracy. Three datasets were collected from our institution for the MR and US image segmentation networks, and the registration network learning, which contained 121, 104, and 63 patient cases, respectively.

Results: The mean Dice similarity coefficient (DSC) results of the two prostate segmentation networks are 0.86 ± 0.05 and 0.90 ± 0.03, for MR images and the US images after the needle insertion, respectively. The mean DSC, center-of-mass (COM) distance, Hausdorff distance (HD), and averaged symmetric surface distance (ASSD) results for the registration of manual prostate contours were 0.87 ± 0.05, 1.70 ± 0.89 mm, 7.21 ± 2.07 mm, 1.61 ± 0.64 mm, respectively. By providing the prostate probability map from the segmentation to the registration network, as well as applying the random map augmentation method, the evaluation results of the four metrics were all improved, such as an increase in DSC from 0.83 ± 0.08 to 0.86 ± 0.06 and from 0.86 ± 0.06 to 0.87 ± 0.05, respectively.

Conclusions: A novel segmentation-based registration framework was proposed to automatically register prostate MR images to the treatment planning US images with metal artifacts, which not only largely saved the labor work on the data preparation, but also improved the registration accuracy. The evaluation results showed the potential of this approach in HDR prostate brachytherapy practice. © *2021 American Association of Physicists in Medicine* [https://doi.org/10.1002/mp.14901]

Key words: deep learning, MR to US image registration, prostate brachytherapy, segmentation, weak supervision

1. INTRODUCTION

Contouring tumors and organs at risk (OARs) in medical images is a prerequisite of radiotherapy. In high dose rate (HDR) brachytherapy procedures, using real-time ultrasound (US) images for the image guidance of the needle insertion and contouring are usually preferred to improve the treatment plan quality. However, the US image is limited by its low tissue contrast, especially in the prostate brachytherapy in which the inserted needles introduce artifacts and degrade the image quality.[1] Compared with the US imaging, the magnetic resonance (MR) imaging could better present the fine structure of soft tissues,[2] and thus

has an advantage in the tumor and OAR contouring process. For example, some intraprostatic lesions are visible on MR images,[3] while it is difficult to identify such lesions on US images.[4] Therefore, delineating contours on the high-quality MR image and then propagating them to the treatment planning US image by using the image registration technology[5] would aid the contouring process in HDR prostate brachytherapy.

Recently, deep learning-based approaches have been proposed to automatize the labor-intensive image registration process.[6–11] In general, paired source (moving) image and target (fixed) image to be registered are fed to the deep learning network, and the corresponding transformation matrix would

be predicted. The moving image could then be transformed with this matrix to generate the registered image. During the network training process, the similarity between the registered image and the fixed image is measured to optimize the network parameters. However, the multi-modality image registration, such as MR to US image registration, is still a challenging task, mainly because it is difficult to measure the image similarity during the optimization process.[12,13] In MR and US images, the same anatomical structure might appear with different image intensity ranges because of the different nature in imaging principles,[13,14] and thus the conventional intensity-based measuring metric utilized in the mono-modality image registration cannot be applied in the multi-modality scenario.[5]

To address this problem, many strategies were studied for multi-modality image registration. Some studies used the supervised method, as the image similarity between the registered and fixed images was evaluated by measuring the difference between the predicted and the ground truth transformation matrixes, while this method was highly limited by the availability and quality of the ground truth matrix.[15–17] The unsupervised method was also investigated in multi-modality registration, as the image similarity was directly measured based on their pixel-level intensity information,[13,18] which was still affected by the limitation as mentioned above. Moreover the weakly-supervised strategy was further proposed to bypass the ground truth transformation and the intensity-based image similarity measure.[19–25] Instead of the pixel-level intensity, high-level labels representing anatomical structures were used to measure the correspondence of multi-modality images. Specifically, anatomical structures were labeled on the moving and fixed images, and the overlap between the transformed label and the corresponding fixed label was measured to evaluate the image similarity and guide the learning process.

Although the weakly-supervised method provides a feasible way for multi-modality image registration, hundreds or thousands of anatomical structures have to be manually contoured on the paired images to be registered for the training process of this label-driven method. This data preparation is labor-intensive and time-consuming,[19,21] and manually contouring also depends on the expert knowledge with interobserver variation,[20] which limits the application of this method in many registration problems.

Recent studies on prostate MR to US image registration are specific to the US image without needle insertion, which is different from the radiation therapy scenario. In HDR brachytherapy procedures, the contouring process is usually finalized after the needle insertion. Therefore, the US imaging used for treatment planning is highly impacted by the stainless steel needles, which would degrade the image quality with severe artifacts, as shown in Fig. 1. It can be seen that the metal artifact dramatically reduces the prostate contrast, and the boundary is blurred after the needle insertion. Therefore, it is more meaningful and challenging to register high-quality images from other modalities to US images with needles for radiation therapy.

To the best of our knowledge, this study first looked at the deep learning-based registration of MR images to the treatment planning US images after the needle insertion for HDR brachytherapy. To address the problem of lacking weak supervision labels and difficulty of accurate registration from inferior image quality, the image segmentation method was employed in this registration study, and a novel deep learning framework was proposed for this challenging task. The registration result was evaluated to show the potential of this approach in HDR prostate brachytherapy.

2. MATERIALS AND METHODS

2.A. Segmentation-based registration framework

In this study, a segmentation-based framework was proposed for the multi-modality prostate image registration, as shown in Fig. 2. Based on the weakly-supervised strategy, the high-level prostate label was used to measure the image similarity after the registration. In this framework, deep learning-based segmentation was used to generate the label automatically for the weakly-supervised registration learning, and thereby manually anatomical label contouring was unnecessary. Two convolutional neural networks were first trained to learn the prostate segmentation on MR and US images separately, and then the two networks were used to generate the prostate probability maps from the MR and US
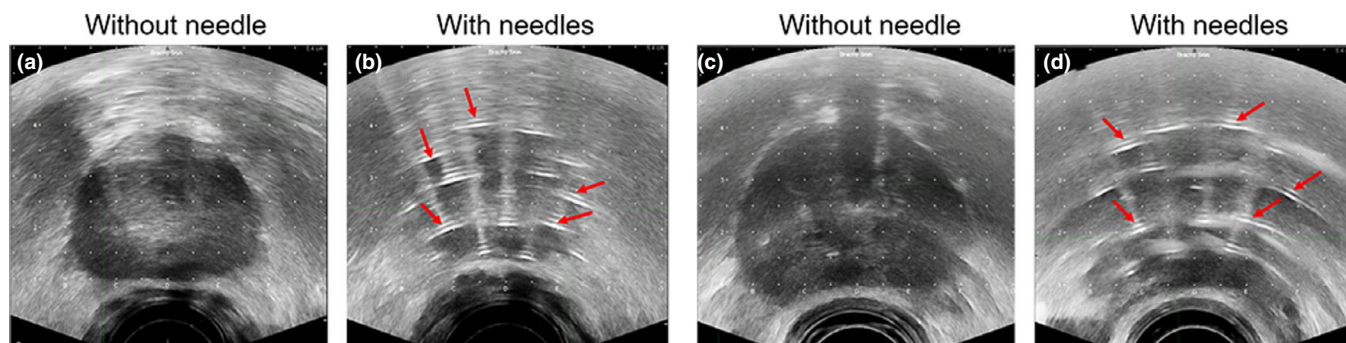

FIG. 1. US images of two patient cases ((a, b) and (c, d), respectively) before and after the needle insertion. Some metal artifacts are indicated by red arrows. [Color figure can be viewed at wileyonlinelibrary.com]
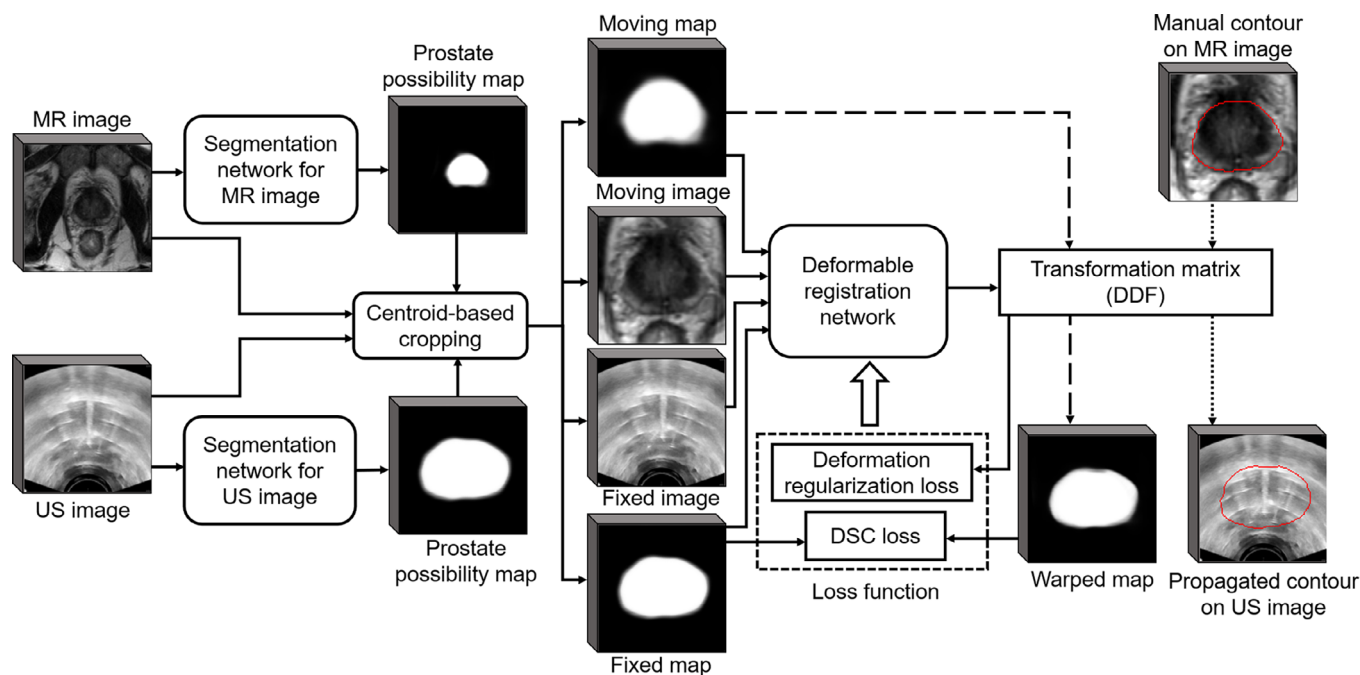
FIG. 2. Framework of the segmentation-based registration approach. [Color figure can be viewed at wileyonlinelibrary.com]

images to be registered as the weak supervision label for the subsequent registration process.

We assumed that the prostate shape information played an important role in this MR to US registration problem, as the prostate was the most distinct anatomical structure in planning US images, and the two prostate volumes in the MR and US images should overlap well after an ideal registration. If we could provide the prostate shape information from the MR and US images to the registration network, it might improve the organ alignment and facilitate the network learning. Therefore, besides the image pair to be registered, we further fed the corresponding prostate probability maps generated from the segmentation to the registration network.

The paired MR and US images and the corresponding prostate probability maps were resized to the same resolution, and cropped to the same size. A preliminary rigid registration was performed by aligning the centroids of the two prostate volumes. Then the cropped image pair and probability map pair were fed to the registration network to generate an output of a pixel-wise transformation matrix for the deformable registration. The transformation matrix was the dense displacement field (DDF)[21] consisting of the displacement distances of each pixel in three orthogonal directions. Thereby, the original MR image (moving image) could be transformed with the DDF to generate the registered image (warped image) to match the US image (fixed image).

During the training process, the prostate probability map from the MR image (moving map) was transformed with the predicted DDF to generate the warped map. Then the overlap between the warped map and the fixed map from the US image was calculated to measure the map similarity and guide the network learning. In the application of this approach in practice, the manual contour in the MR image could be transformed using the predicted DDF to generate the propagated contour in the US image, which would be used in the treatment planning of HDR brachytherapy.

2.B. Sub-networks

In this work, a widely used 3D V-Net[26] was applied to the segmentation of the prostate on MR and US images, with commonly implemented batch normalization (BN)[27] and a dropout[28] of 0.5. Two segmentation networks were trained for MR and US images separately, with the same network structure and different parameter values. The whole 3D image volume was input to the network, and the pixel-wise probability map of the prostate was output by the Softmax activation function in the last layer. The predicted prostate probability map was compared with the manual prostate contour to calculate the Dice loss[29] for the network parameter optimization. Once the two networks were trained, they were used to predict the prostate probability maps from the MR and US images to be registered, for the subsequent registration training and prediction.

A 3D U-Net like network from Hu et al.[19] was used for the deformable transformation (Fig. 3). It consisted of four down-sampling layers, one bottleneck layer, and four up-sampling layers, and was more densely connected than the U-Net proposed for image segmentation.[30] The input of this network was a combination of paired MR and US images, as well as the corresponding prostate probability maps. The DDF for the deformable registration was output, which could then transform the moving image or probability map to the registered one.
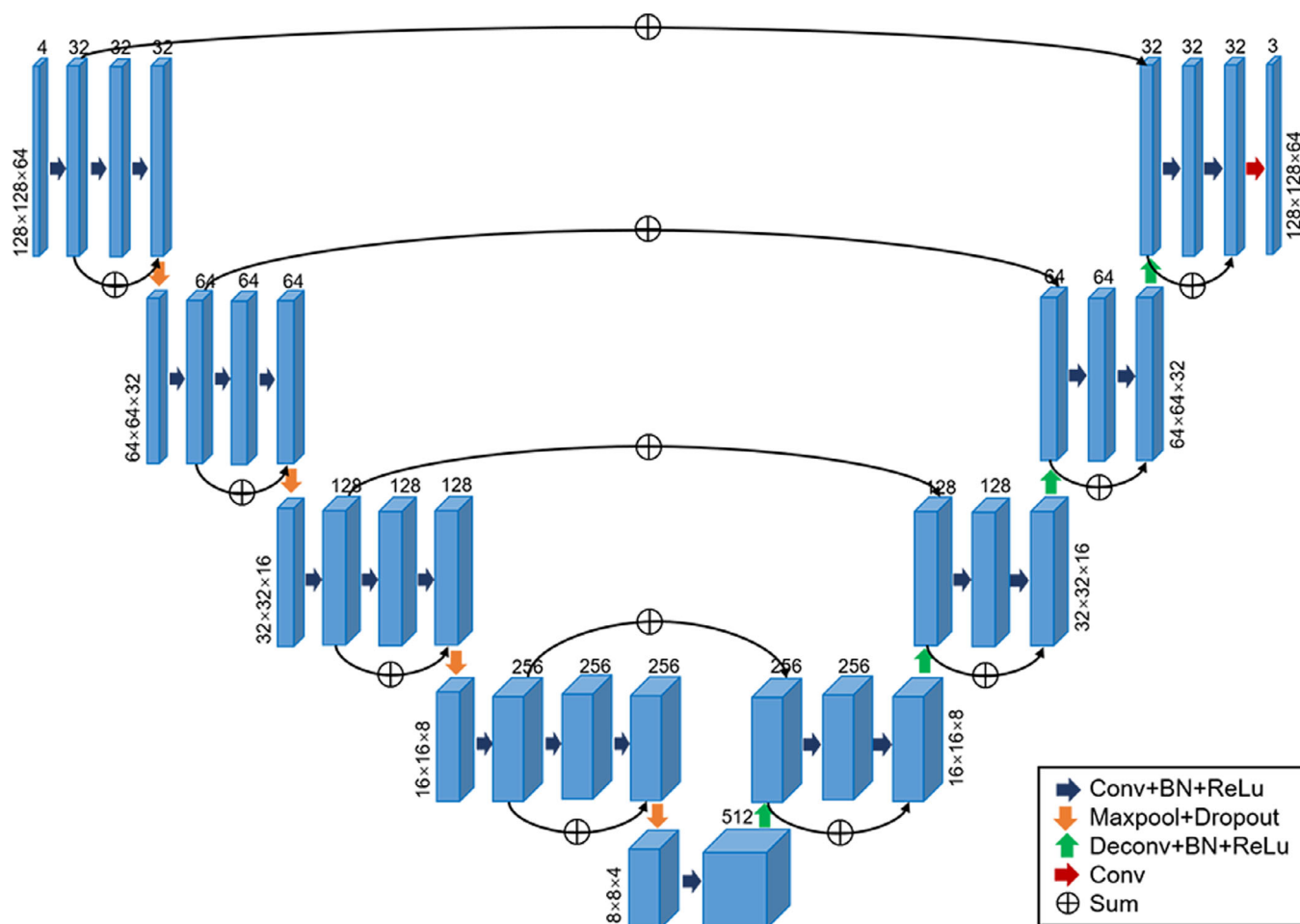
Fig. 3. Architecture of the deformable registration network. [Color figure can be viewed at wileyonlinelibrary.com]

2.C. Datasets and processing

In this study, three datasets from our clinical database with Institutional Review Board approval (IRB 41755) were prepared for the two segmentation networks and one registration network. The segmentation dataset consisted of images with prostate contours, and there were already many relevant databases available for this purpose.[31–33] The registration dataset contained paired MR and US images to be registered, and the manual label was unnecessary for the network training.

As for the MR dataset for segmentation, we utilized our previous database originally for intraprostatic lesion segmentation,[34] in which the prostate and intraprostatic lesions were manually contoured on multi-modality MR images. The T2W images with prostate contours of 121 patient cases in this database were used for the prostate segmentation on MR images in this study. All the images and prostate masks were resized to a size of $128 \times 128 \times 64$ with an in-plane resolution of 0.92 mm. We collected US images with manual contours of 104 patient cases from our institution. The US images were acquired during the HDR brachytherapy procedure using the Vitesse software (Varian Medical Systems, Inc., Palo Alto, CA) with a pixel size of $(0.10–0.14) \times (0.10–0.14) \times 1.0$ mm^3 and in-plane size of 580×600 pixel. Prostates were manually contoured by radiation oncologists for treatment planning. The US images and masks were resized to a size of $128 \times 128 \times 64$ with an in-plane resolution of 0.46 mm. All the MR and US images were normalized to zero-mean with unit-variance intensities.

The registration dataset included paired MR and US images from 63 cases of 53 patients, as some patients received two brachytherapy treatments with two US scans. Some imaging parameters of the MR images were as follows: magnetic field strength = 3T; repetition time = 3170–10165 ms; echo time = 85–149 ms; flip angle = 90°–160°; slice thickness = 2.5–4.2 mm; in-plane resolution = 0.3125–0.625 mm. The US images were also acquired using the Vitesse software with a pixel size of $(0.10–0.14) \times (0.10–0.14) \times 1.0$ mm^3 and in-plane size of 580×600 or 501×1028 pixel. Prostates were manually contoured on 11 cases from 11 patients as the testing set, to evaluate the accuracy of this approach on the propagation of ground truth contours. The paired MR and US images were first fed to the trained segmentation networks to generate the prostate probability maps. Then both the images and probability maps were resized to the same resolution of

$0.46 \times 0.46 \times 0.95$ mm^3 and cropped to the same size of $128 \times 128 \times 64$ before being input to the registration network.

2.D. Implementation details

For the MR image segmentation, 100 patient cases were used for the training, 21 for the validation. For the US image segmentation, 82 cases were used for the training, 22 for the validation. For the registration, 40 cases from 33 patients were used for the training, 12 cases from 9 patients for the validation, and 11 cases from 11 patients for the testing. During the segmentation and registration training, data augmentation was applied to alleviate the overfitting problem with various image transformations, including randomly shifting with the range $(-5\%, 5\%)$ of the image size in width and height directions, and horizontal and vertical flipping with 50% and 10% probabilities separately. The adaptive moment (Adam) algorithm[35] was applied to optimize the parameter of all the three networks. All computations for learning were performed on an NVIDIA GeForce RTX 2080 Ti GPU with 11GB memory.

Exclusively for the registration learning, the spatial transformation network (STN)[36] provided by the Pytorch was used to transform images or prostate probability maps with the predicted DDF. The overlap between the warped and fixed probability maps was measured with a soft Dice loss function:[37]

$$L_{\text{Dice}} = 1 - \frac{2\sum_{p \in V} w_p \cdot f_p}{\sum_{p \in V} w_p^2 + \sum_{p \in V} f_p^2} \tag{1}$$

where w_p and f_p denote the prostate probability values in pixel p in the warped and fixed maps, and V denotes the whole image volume. Since Dice loss alone might generate a non-smooth DDF that is not physically plausible, regularization of the deformation field was necessary. Thus an L^2-norm[38] was used on the spatial gradient of the DDF d to encourage a smooth deformation:

$$L_{\text{smooth}} = \frac{1}{V} \sum_{p \in V} \| \nabla \mathbf{d}(p) \|^2 \tag{2}$$

Therefore, a combined Dice and weighted L^2 regularization loss function was used to train the registration network:

$$L_{\text{total}} = L_{\text{Dice}} + \lambda L_{\text{smooth}} \tag{3}$$

where λ is a regularization weight parameter.

Since the prostate probability maps were used as the inputs and weak supervision labels simultaneously, the network might learn to align only the two maps, while bypassing the whole image registration. Therefore, the input and label maps would better vary during the training process to alleviate this map overfitting problem, and a map augmentation method was further designed. Specifically, the pixel probability value was randomly scaled for each input and label probability map separately. Since probability value p_i in pixel i should be in the range of $[0, 1]$, all the p_i were adjusted using Eq. (4) to generate the scaled probability p_{si}:

$$p_{si} = p_i^{\gamma} \tag{4}$$

The power γ was uniformly sampled from a range for each probability map during the training. The range value was regarded as a hyperparameter in this study, and selected as $[0.3, 1.7]$ after the trial. Thereby, the two inputting probability maps, as well as the two label maps were all different from each other after this augmentation, to alleviate the overfitting problem when utilizing the probability maps for registration training. Two example probability maps with different scaling are shown in Fig. 4.
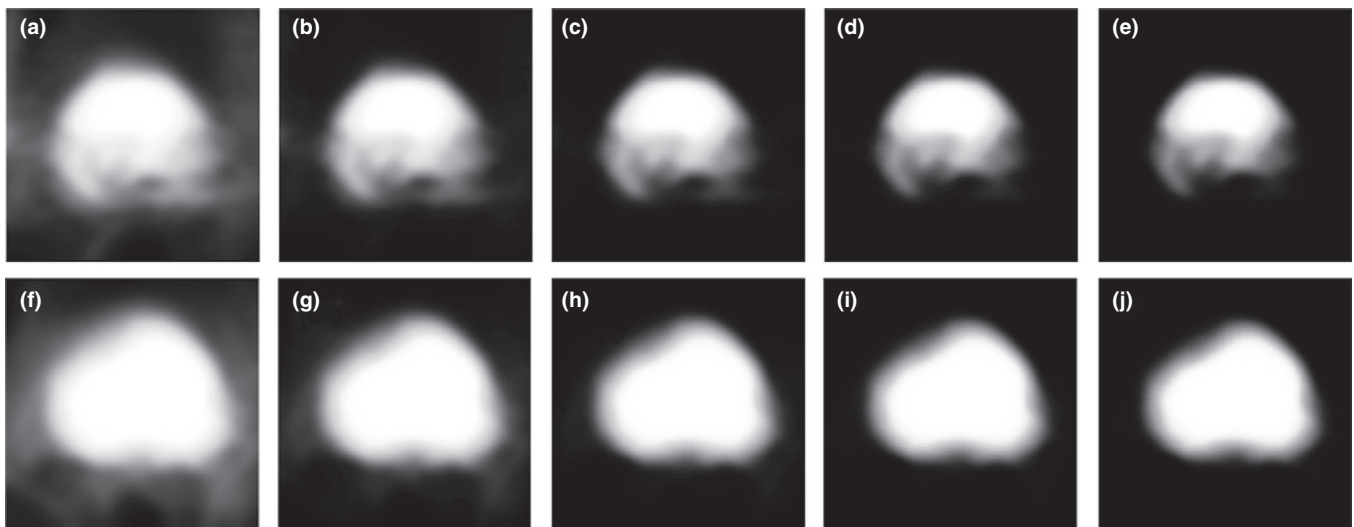

FIG. 4. Two example prostate probability maps scaled with different γ values. (a) and (f): $\gamma = 0.3$; (b) and (g): $\gamma = 0.6$; (c) and (h): $\gamma = 1.0$; (d) and (i): $\gamma = 1.4$; (e) and (j): $\gamma = 1.7$.

2.E. Evaluation metrics

In this work, the Dice similarity coefficient (DSC) was used as the main metric to evaluate the segmentation accuracy, as well as the precision and sensitivity.[39] The three metrics are defined as follows:

$$Dice = \frac{2|G \cap P|}{|G| + |P|} \quad (5)$$

$$Precision = \frac{|G \cap P|}{|P|} \quad (6)$$

$$Sensitivity = \frac{|G \cap P|}{|G|} \quad (7)$$

where G and P denote the ground truth and the predicted segmentation of the prostate.

To evaluate the registration accuracy of this approach, DSC was also used to measure the spatial overlap between the warped prostate volume and the fixed one. And center-of-mass (COM) distance[40] was evaluated, which was defined as the distance between the centroids of the registered and fixed prostate volumes in this study. Hausdorff distance (HD) and averaged symmetric surface distance (ASSD) were also used to evaluate the largest and average surface distances between the warped and fixed prostate volumes,[41] respectively.

3. RESULTS

The two segmentation networks were trained using the MR and US segmentation datasets separately, and the evaluation results on the testing set of the registration dataset are shown in Table I. To evaluate the prediction accuracy of the registration network, we first analyzed the registration of the segmentation network-predicted prostate masks from the MR and US images. Since the manual prostate contour could be regarded as the ground truth representing the real prostate boundary, the registration of the manual contours delineated on the MR and US images was further investigated, which was closer to the clinical application scenario. The evaluation results for the two registration targets on the testing set are shown in Table II, labeled as "Segmented mask" and "Manual contour," respectively. Before the deformable registration process, the MR and US images were cropped to align the centroids of the two segmented prostate volumes, which could be regarded as a preliminary rigid registration. The evaluation result of this preliminary registration only based on the segmentation result was also compared in Table II.

TABLE I. Evaluation results (mean value $\pm$ standard deviation) of the two segmentation networks on the testing set.

Image modality	DSC	Precision	Sensitivity
MR	0.86 ± 0.05	0.87 ± 0.07	0.87 ± 0.12
US	0.90 ± 0.03	0.85 ± 0.06	0.95 ± 0.02

MR, magnetic resonance; US, ultrasound; DSC, Dice similarity coefficient.

TABLE II. Evaluation results (mean value $\pm$ standard deviation) for the segmented prostate mask and manual contour before and after the deformable registration.

Evaluation metric	Before the deformable registration		After the deformable registration	
	Segmented mask	Manual contour	Segmented mask	Manual contour
DSC	0.83 ± 0.05	0.80 ± 0.07	0.97 ± 0.00	0.87 ± 0.05
COM (mm)	0.09 ± 0.29	2.00 ± 0.91	0.15 ± 0.16	1.70 ± 0.89
HD (mm)	8.17 ± 2.46	9.02 ± 2.79	2.05 ± 0.38	7.21 ± 2.07
ASSD (mm)	2.23 ± 0.68	2.42 ± 0.81	0.38 ± 0.02	1.61 ± 0.64

DSC, Dice similarity coefficient; COM, center-of-mass; HD, Hausdorff distance; ASSD, averaged symmetric surface distance.

It can be seen that the centroid-based preliminary registration achieves a DSC result of 0.80 ± 0.07 for the manual contours alignment, which is comparable to a deep learning-based affine registration result of 0.73 in a similar study.[21] After the deformable registration, the evaluation results of the four metrics were all further improved, both for the registration of the segmented mask and manual contour. For example, there are about 0.14 and 0.07 DSC increase for the two registration targets, respectively. The evaluation results for the segmented mask were better than those for the manual contour, as the network was trained under the weak supervision of the prostate probability map from the segmentation, while the manual contour was only used in the evaluation.

Since some similar studies, such as Hu et al.[19] and Zeng et al,[20] used paired images or prostate binary masks as the input of the registration network, the impact of the input data on the registration prediction result was further investigated. The evaluation results for the manual contour registration with the input of the MR and US image pair, the prostate probability map pair, and the combination of the image pair and map pair are compared in Table III. The effect of the prostate probability map augmentation during the training process was also analyzed, by which the probabilities of all the pixels in each map were randomly scaled to alleviate the map overfitting. The evaluation results of inputting the map pair, and the combination of the image pair and map pair are both better than only feeding the image pair to the network. It indicates that the prostate probability map generated by the segmentation network could help the registration network learning and promote the prediction result, such as an increase in DSC from 0.83 ± 0.08 to 0.86 ± 0.06, and a decrease in ASSD from 2.10 ± 0.94 mm to 1.72 ± 0.77 mm. When applying the map augmentation described above, all the evaluation results are further improved, showing the efficiency of this method in the segmentation-based registration.

Figure 5 presents three examples for the registration of the manual prostate contour by this deep learning approach, and the registered contour from the MR image was compared with the fixed one on the US image. It shows that the warped

TABLE III. Comparison of the manual contour registration results (mean value ± standard deviation) with different input data, as well as using the prostate probability map augmentation. The paired two-tailed t-test was used between the results of the proposed method (last column) and the other comparing methods.

Evaluation metric	Image input	Map input	Image and map inputs	Image and map inputs with map augmentation
DSC				
Result	0.83 ± 0.08	0.86 ± 0.07	0.86 ± 0.06	0.87 ± 0.05
P-value	0.007	0.028	0.029	—
COM (mm)				
Result	1.93 ± 0.69	1.83 ± 0.89	1.78 ± 0.92	1.70 ± 0.89
P-value	0.159	0.085	0.290	—
HD (mm)				
Result	8.41 ± 2.41	7.80 ± 2.40	7.85 ± 2.42	7.21 ± 2.07
P-value	0.013	0.044	0.030	—
ASSD (mm)				
Result	2.10 ± 0.94	1.72 ± 0.78	1.72 ± 0.77	1.61 ± 0.64
P-value	0.015	0.071	0.082	—

DSC, Dice similarity coefficient; COM, center-of-mass; HD, Hausdorff distance; ASSD, averaged symmetric surface distance.

contours match well with the fixed contours in the axial, sagittal, and coronal views, indicating the potential of this approach in automatic contour propagation.

Although this study mainly paid attention to the contour propagation from the high-quality MR image to the low-quality US image, the registration performance in terms of deformation rationality on the image level, which was the basis of the contour propagation, was also investigated. Example axial slices of the original MR images, registered MR images, and fixed US images from three patient cases are shown in Fig. 6 for qualitative visual assessment. It indicates that the overall MR image deformation is visually realistic, and the propagated contours are also closer to the contours on the fixed US images than the unregistered ones.

4. DISCUSSION

This study first worked on the deep learning-based registration for the treatment planning US image, in which the image quality was highly degraded by the severe artifacts from the metal needles. Although this registration task is challenging, it is clinically significant for HDR brachytherapy, as OARs are actually contoured on the planning US image and the corresponding automatic registration is needed in clinical practice. To better address the difficulty encountered in this multi-modality image registration procedure, a segmentation-based registration framework was proposed in this study.

As one of the main methods in deep learning-based multi-modality registration, the weakly-supervised method depends on a large amount of paired anatomical labels on the paired
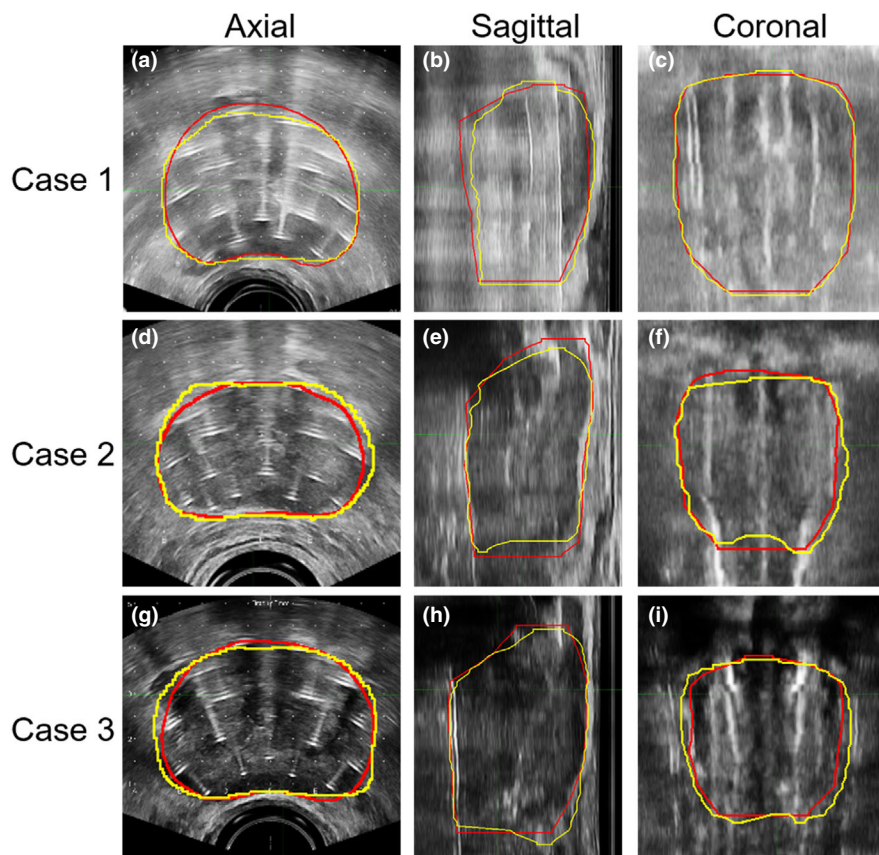

FIG. 5. Comparison of the registered (yellow color) and fixed (red color) manual prostate contours in three patient cases. The three columns are for the axial, sagittal, and coronal views separately. [Color figure can be viewed at wileyonlinelibrary.com]

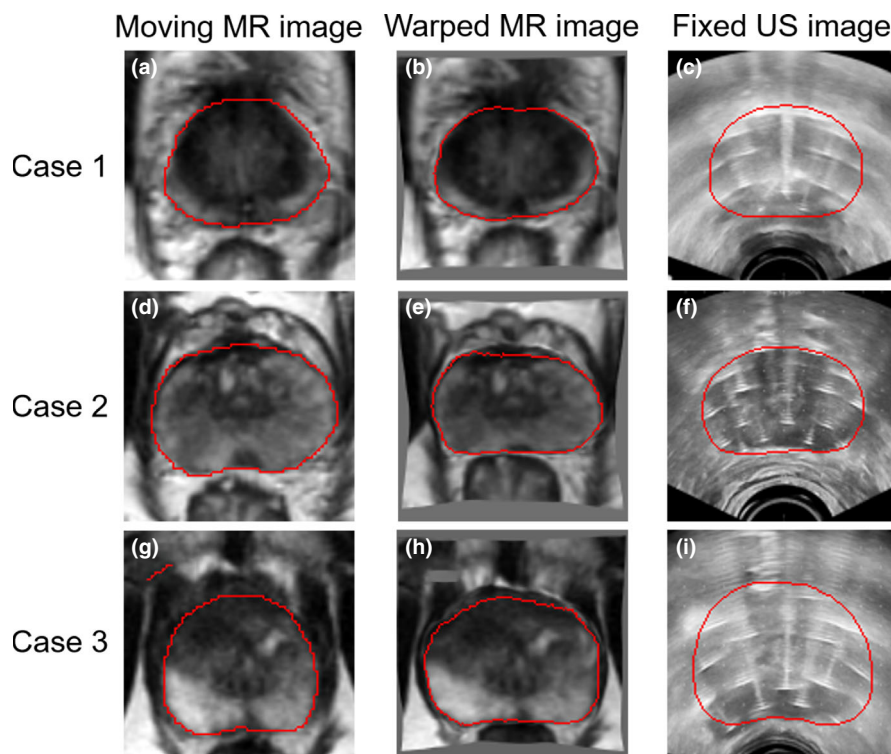Moving MR image   Warped MR image   Fixed US image

FIG. 6. Comparison of the moving MR images (in the first column with manual contours), warped MR images after the deformable registration (in the second column with warped contours), and fixed US images (in the last column with manual contours) from three patient cases. All the three in-plane images of each patient case are corresponding to the same location in superior-inferior direction in the cropped image volume. The prostate contours are in red color. [Color figure can be viewed at wileyonlinelibrary.com]

images to be registered. We used the deep learning method to automatically generate those labels on the MR and US images, to ease the data limitation in this registration study. In the proposed framework, the paired labels were output by the two segmentation networks, and it was unnecessary to label on the paired MR and US images manually, which largely reduced the labor work on the data preparation. Although anatomical labels were also needed for the segmentation network training, the corresponding MR and US datasets could be from two different patient groups, which largely extended the source of the data, and then many relevant datasets can be utilized. The proposed segmentation-based registration framework could be applied to not only this prostate MR to US registration task, but also some other multimodality registration problems where the label data is the bottleneck.

In this study, the US images with severe metal artifacts and blurred organ boundaries highly increased the difficulty of accurate registration. Since the same organ in the paired images should fully overlap after an ideal registration, we considered providing some organ shape information to the registration network along with the image pair to facilitate the network learning. Although the images also contained the organ shape information, it might be difficult for the registration network to extract such information well without strong supervision. By providing the two prostate probability maps from the segmentation to the registration network, along with the designed map augmentation method to alleviate the map

overfitting during the training process, the registration results in terms of DSC, COM, HD, and ASSD were all improved, demonstrating the effect of our methods in this registration problem.

Some other studies also worked on the registration of prostate MR images to US images using the weakly-supervised strategy. For example, Hu et al.[19] and Zeng et al.[20] achieved mean DSCs of 0.87 and 0.91 on the prostate contour propagation respectively, which were higher than our result. In this study, the DSC results of the two prostate segmentation networks were both less than 0.9, and thus there was some shape difference between the segmented and manually contoured prostate volumes. Since the registration network was trained under the weak supervision of the segmented prostate probability map, the registration results for the manual contour were lower than those for the segmented mask. Some other weakly-supervised approaches used manual contours for network training and evaluation, and thus the registration evaluation result tended to be better because of using the ground truth contour as the supervision label. Moreover it is more difficult for the network to learn the transformation matrix from the low-quality US images after the needle insertion, and thus the evaluation result of this study was relatively lower.

As far as we know, this is also the first study to examine deep learning-based prostate segmentation on the US image after the needle insertion. Even with the inferior image quality, the DSC result of this segmentation is close to some other studies focusing on the US image without the needle

insertion.[29,42,43] Metal needles are usually distinct in US images, and often uniformly distributed within the prostate. Although prostate boundaries are blurred in these images, the needle signals could serve as another prostate location and shape information, which might help the network learning.

This study still has much room for improvement. Since we did not focus on the sub-network refining, and only a regular 3D V-Net was used for the prostate segmentation, the DSC result was lower than some state-of-art networks, which further had a negative impact on the subsequent registration process. Therefore, a more sophisticated network would be developed for the segmentation task to improve the final registration result. Because of the impact of the metal artifact in planning US images, it is difficult to manually label other anatomical structures in the paired images for the evaluation of registration accuracy, and only the prostate contour was utilized at current stage. In the future, more anatomical structure contours would be used for a better evaluation of this registration approach. Limited by the current dataset, only 52 cases were used for the training and validation, and 11 cases for the evaluation. Because of the low number of testing cases, the generalization of this deep learning study remains to be investigated, and more image data will be collected in the future study.

Biomechanical constraint method was previously used in surface-based registration of prostate MR and US images,[44,45] which utilized the finite element analysis to regularize the deformation matrix to be physically plausible, especially for the internal prostate deformation. Recently, Fu et al.[46] and Hu et al.[47] applied the biomechanical constraint idea to the deep learning-based image registration to improve the registration accuracy. Since less anatomical structures could be labeled on planning prostate US images for weakly-supervised learning, the accuracy of the predicted deformation within the prostate remains to be improved. Therefore, biomechanically constrained registration would be a future development direction in this registration problem.

In current HDR brachytherapy practice in our institution, the prostate MR image is manually rigidly registered to the US image by using the prostate contours in the two images as a reference. Since there would be some organ distortion and movement between the two images, only using rigid registration could not compensate this shape difference. This study provided an automatic approach for this image registration task, and the adopted deformable registration method could help to correct the difference of the organ shapes. In a previous study,[34] we worked on the automatic segmentation of intraprostatic lesions on MR images, and then the lesion contours could be automatically propagated to the planning US images during the HDR brachytherapy procedure, allowing for dose escalation to specific intraprostatic lesions if warranted.

5. CONCLUSIONS

In this study, a deep learning approach was first applied to register prostate MR images to the treatment planning US images after the needle insertion. To address the problem of lacking weak supervision labels and difficulty of accurate registration from inferior image quality, a new segmentation-based registration framework was proposed by employing the deep learning-based segmentation method in the registration study. This framework not only largely saved the labor work on the data preparation, but also improved the registration accuracy, which could also be applied to other multi-modality registration problems. The evaluation results show the registration of high-quality MR images and planning US images with severe metal artifacts could be realized with this deep learning framework, and its potential to be used in HDR prostate brachytherapy to automatize current clinical procedures.

CONFLICT OF INTEREST

The authors have no relevant conflicts of interest to disclose.

Data Availability Statement

The datasets from Stanford Hospital are protected because of patient privacy. They may be available upon request provided that approval is obtained after an Institutional Review Board procedure at Stanford.

a)Author to whom correspondence should be addressed. Electronic mail: hanbin@stanford.edu.

REFERENCES

1. Wang F, Xing L, Bagshaw H, Buyyounouski M, Han B. Deep learning applications in automatic needle segmentation in ultrasound-guided prostate brachytherapy. _Med Phys_. 2020;47:3797–3805.
2. Orlando N, Gillies DJ, Gyacskov I, Romagnoli C, D'Souza D, Fenster A. Automatic prostate segmentation using deep learning on clinically diverse 3D transrectal ultrasound images. _Med Phys_. 2020;47:2413–2426.
3. Turkbey B, Rosenkrantz AB, Haider MA, et al. Prostate imaging reporting and data system version 2.1: 2019 update of prostate imaging reporting and data system version 2. _Eur Urol_. 2019;76:340–351.
4. Kaushal R, Das CJ, Singh P, Dogra PN, Kumar R. Multiparametric magnetic resonance imaging-transrectal ultrasound fusion biopsies increase the rate of cancer detection in populations with a low incidence of prostate cancer. _Invest Clin Urol_. 2019;60:156–161.
5. Thor M, Petersen JB, Bentzen L, Høyer M, Muren LP. Deformable image registration for contour propagation from CT to cone-beam CT scans in radiotherapy of prostate cancer. _Acta Oncol_. 2011;50:918–925.
6. Fu Y, Lei Y, Wang T, Curran WJ, Liu T, Yang X. Deep learning in medical image registration: a review. _Phys Med Biol_. 2020;65:20TR01.
7. Haskins G, Kruger U, Yan P. Deep learning in medical image registration: a survey. _Mach Vis Appl_. 2020;31:8.
8. de Vos BD, Berendsen FF, Viergever MA, Sokooti H, Staring M, Išgum I. A deep learning framework for unsupervised affine and deformable image registration. _Med Image Anal_. 2019;1:128–143.

9. Fu Y, Lei Y, Zhou J, et al. Non-rigid MRI-CT image registration with unsupervised deep learning-based deformation prediction. In Medical Imaging 2020: Image Processing (Vol. 11313, p. 1131329). International Society for Optics and Photonics. 2020.

10. Cao X, Yang J, Wang L, Xue Z, Wang Q, Shen D. Deep learning based inter-modality image registration supervised by intra-modality similarity. In International Workshop on Machine Learning in Medical Imaging. Cham: Springer; 2018:55–63.

11. Zhu N, Najafi M, Han B, Hancock S, Hristov D. Feasibility of image registration for ultrasound-guided prostate radiotherapy based on similarity measurement by a convolutional neural network. *Technol Cancer Res Treat*. 2019;19:1533033818821964.

12. Haskins G, Kruecker J, Kruger U, et al. Learning deep similarity metric for 3D MR–TRUS image registration. *Int J Comput Assist Radiol Surg*. 2019;14:417–425.

13. Sun L, Zhang S. Deformable MRI-ultrasound registration using 3d convolutional neural network. In Simulation, Image Processing, and Ultrasound Systems for Assisted Diagnosis and Navigation. Cham: Springer; 2018:152–158.

14. Qin C, Shi B, Liao R, Mansi T, Rueckert D, Kamen A. Unsupervised deformable registration for multi-modal images via disentangled representations. In International Conference on Information Processing in Medical Imaging. Cham: Springer; 2019:249–261.

15. Yan P, Xu S, Rastinehad AR, Wood BJ. Adversarial image registration with application for MR and TRUS image fusion. In International Workshop on Machine Learning in Medical Imaging. Cham: Springer; 2018:197–204.

16. Rohé MM, Datar M, Heimann T, Sermesant M, Pennec X SVF-Net: Learning deformable image registration using shape matching. In International conference on medical image computing and computer-assisted intervention. Cham: Springer; 2017:266–274.

17. Bhardwaj A, Park JS, Mukhopadhyay S, et al. Rigid and deformable corrections in real-time using deep learning for prostate fusion biopsy. In Medical Imaging 2020: Image-Guided Procedures, Robotic Interventions, and Modeling (Vol. 11315, p. 113151W). International Society for Optics and Photonics. 2020.

18. Ferrante E, Oktay O, Glocker B, Milone DH. On the adaptability of unsupervised CNN-based deformable image registration to unseen image domains. In International Workshop on Machine Learning in Medical Imaging. Cham: Springer; 2018:294–302.

19. Hu Y, Modat M, Gibson E, et al. Weakly-supervised convolutional neural networks for multimodal image registration. *Med Image Anal*. 2018;1:1–3.

20. Zeng Q, Fu Y, Tian Z, et al. Label-driven magnetic resonance imaging (MRI)-transrectal ultrasound (TRUS) registration using weakly supervised learning for MRI-guided prostate radiotherapy. *Phys Med Biol*. 2020;65:135002.

21. Hu Y, Modat M, Gibson E, et al. Label-driven weakly-supervised learning for multimodal deformable image registration. In 2018 IEEE 15th International Symposium on Biomedical Imaging (ISBI 2018). 2018:1070–1074.

22. Hu Y, Gibson E, Ghavami N, et al. Adversarial deformation regularization for training image registration neural networks. In International Conference on Medical Image Computing and Computer-Assisted Intervention. Cham: Springer; 2018:774–782.

23. Zeng Q, Fu Y, Jeong J, et al. Weakly non-rigid MR-TRUS prostate registration using fully convolutional and recurrent neural networks. In Medical Imaging 2020: Image Processing (Vol. 11313, p. 113132Y). International Society for Optics and Photonics. 2020.

24. Hering A, Kuckertz S, Heldmann S, Heinrich MP. Enhancing label-driven deep deformable image registration with local distance metrics for state-of-the-art cardiac motion tracking. In Bildverarbeitung für die Medizin. Wiesbaden: Springer Vieweg; 2019:309–314.

25. Balakrishnan G, Zhao A, Sabuncu MR, Guttag J, Dalca AV. Voxel-Morph: a learning framework for deformable medical image registration. *IEEE Trans Med Imaging*. 2019;38:1788–1800.

26. Milletari F, Navab N, Ahmadi SA. V-net Fully convolutional neural networks for volumetric medical image segmentation. In 2016 fourth international conference on 3D vision (3DV) 2016 (pp. 565–571). IEEE.

27. Ioffe S, Szegedy C. Batch normalization: Accelerating deep network training by reducing internal covariate shift. arXiv preprint arXiv: 1502.03167. 2015.

28. Srivastava N, Hinton G, Krizhevsky A, Sutskever I, Salakhutdinov R. Dropout: a simple way to prevent neural networks from overfitting. *J Mach Learning Res*. 2014;15:1929–1958.

29. Lei Y, Tian S, He X, et al. Ultrasound prostate segmentation based on multidirectional deeply supervised V-Net. *Med Phys*. 2019;46:3194–3206.

30. Ronneberger O, Fischer P, Brox T. U-net: Convolutional networks for biomedical image segmentation. In International Conference on Medical image computing and computer-assisted intervention. Cham: Springer; 2015:234–241.

31. Litjens G, Toth R, van de Ven W, et al. Evaluation of prostate segmentation algorithms for MRI: the PROMISE12 challenge. *Med Image Anal*. 2014;18:359–373.

32. Litjens G, Debats O, Barentsz J, Karssemeijer N, Huisman H. ProstateX challenge data. *Cancer Imaging Archive*. 2017;10:K9TCIA.

33. Bloch N, Madabhushi A, Huisman H, et al. NCI-ISBI 2013 challenge: automated segmentation of prostate structures. *Cancer Imaging Archive*. 2013;2015:370.

34. Chen Y, Xing L, Yu L, Bagshaw H, Buyyounouski M, Han B. Automatic intraprostatic lesion segmentation in multiparametric magnetic resonance images with proposed multiple branch UNet. *Med Phys*. 2020;47:6421–6429.

35. Kingma DP, Adam BJ. A method for stochastic optimization. arXiv preprint arXiv: 1412.6980. 2014.

36. Jaderberg M, Simonyan K, Zisserman A. Spatial transformer networks. In Advances in neural information processing systems 2015 (pp. 2017-2025).

37. Kodym O, Španěl M, Herout A, Segmentation of head and neck organs at risk using cnn with batch dice loss. In German Conference on Pattern Recognition. Cham: Springer; 2018:105–114.

38. Vishnevskiy V, Gass T, Szekely G, Tanner C, Goksel O. Isotropic total variation regularization of displacements in parametric image registration. *IEEE Trans Med Imaging*. 2017;36:385–395.

39. Sajid S, Hussain S, Sarwar A. Brain tumor detection and segmentation in MR images using deep learning. *Arab J Sci Eng*. 2019;44:9249–9261.

40. Kumarasiri A, Siddiqui F, Liu C, et al. Deformable image registration based automatic CT-to-CT contour propagation for head and neck adaptive radiotherapy in the routine clinical setting. *Med Phys*. 2014;41:121712.

41. Yeghiazaryan V, Voiculescu ID. Family of boundary overlap metrics for the evaluation of medical image segmentation. *J Med Imaging*. 2018;5:015006.

42. Lei Y, Wang T, Wang B, et al. Ultrasound prostate segmentation based on 3D V-Net with deep supervision. In Medical Imaging 2019: Ultrasonic Imaging and Tomography (Vol. 10955, p. 109550V). International Society for Optics and Photonics. 2019.

43. Ghavami N, Hu Y, Bonmati E, et al. Automatic slice segmentation of intraoperative transrectal ultrasound images using convolutional neural networks. In Medical Imaging 2018: Image-Guided Procedures, Robotic Interventions, and Modeling (Vol. 10576, p. 1057603). International Society for Optics and Photonics. 2018.

44. van de Ven WJ, Hu Y, Barentsz JO, Karssemeijer N, Barratt D, Huisman HJ. Biomechanical modeling constrained surface-based image registration for prostate MR guided TRUS biopsy. *Med Phys*. 2015;42:2470–2481.

45. Khallaghi S, Sanchez CA, Rasoulian A, et al. Biomechanically constrained surface registration: application to MR-TRUS fusion for prostate interventions. *IEEE Trans Med Imaging*. 2015;34:2404–2414.

46. Fu Y, Lei Y, Wang T, et al. Biomechanically constrained non-rigid MR-TRUS prostate registration using deep learning based 3D point cloud matching. *Med Image Anal*. 2020;7:101845.

47. Hu Y, Gibson E, Ghavami N, et al. Adversarial deformation regularization for training image registration neural networks. In International Conference on Medical Image Computing and Computer-Assisted Intervention. Cham: Springer; 2018:774–782.